Cluster folding analysis for ^{15}N ions scattered by ^{13}C and ^{27}Al targets

B. Mauyey[a,b], D. Soldatkhan[a], and Sh. Hamada[c,*]

[a] *L.N. Gumilyov Eurasian National University, 010008 Astana, Kazakhstan.*
[b] *Flerov Laboratory of Nuclear Reactions, JINR, 141980 Dubna, Russia.*
[c] *Faculty of Science, Tanta University, Tanta, Egypt.*
[*] *e-mail: sh.m.hamada@science.tanta.edu.eg*

Received 13 August 2024; accepted 20 September 2024

Motivated by two well-known cluster structures for the ^{15}N nucleus, ^{11}B $+\alpha$ and ^{13}C $+d$, which appear at excitation energies of 10.992 and 16.159 MeV, respectively, the angular distributions (ADs) for ^{15}N nuclei elastically scattered in the field of two medium-mass targets, namely, ^{27}Al and ^{13}C are investigated within the cluster folding model. Reasonable agreement between the measured and calculated ADs data for the considered nuclear systems is obtained, which validates the cluster structure description of the ^{15}N ground state, configured as a core (11B/13C) with a valence particle (α/d) orbiting the core. We aim to quantitatively investigate the ^{11}B $+\alpha$ and ^{13}C $+d$ cluster structures of the ground state of the ^{15}N nucleus, providing new insights into fundamental nuclear interactions.

Keywords: Elastic transfer; optical model; folding potential; spectroscopic factor.

DOI: https://doi.org/10.31349/RevMexFis.71.021201

1. Introduction

Nuclear processes initiated by ^{15}N ions [1-5] encompass a broad spectrum of phenomena within nuclear physics. Experimental studies [6-8] have provided significant insights into the interactions of ^{15}N ions with ^{27}Al and ^{13}C target nuclei, shedding light on various reaction channels and their associated cross sections. These processes include elastic scattering, transfer reactions, and inelastic scattering, each offering unique ways to investigate nuclear structure and dynamics. Notably, the collision of ^{15}N ions with target nuclei has demonstrated intriguing phenomena such as clusterization effects and anomalous scattering patterns, prompting theoretical investigations into their underlying mechanisms. Furthermore, the use of ^{15}N ions as projectiles has facilitated the study of nucleon-nucleon interactions and the spectroscopic properties of target nuclei, with applications ranging from fundamental nuclear physics research to practical implications in fields such as nuclear energy and astrophysics.

At energies close to the Coulomb barrier, the repulsion caused by the Coulomb force between two nuclei is extremely strong, leading to a range of fascinating phenomena, such as nucleon(s) transfer, that are not observed at higher energies. The study of nuclear clustering is a crucial area of focus in this field. Nuclear clustering involves the formation of clusters within a nucleus, consisting of a precise number of nucleons. These clusters usually form from stable nuclei or their individual components. Investigating nuclear processes involving clusterized nuclei provides new insights into the structure, characteristics, and interactions of the nucleus. At energies near the Coulomb barrier, the nuclei are not moving fast enough to fully overcome the Coulomb repulsion, but they are close enough that nuclear effects become significant. At these energies, the interaction between nuclei can lead to more complex nuclear phenomena. Specifically, the strong electrostatic repulsion is counteracted by the nuclear forces, which can promote the formation of clusters or composite structures inside the nuclei [9].

The cornerstone concept for the description of a nucleus is that independent nucleons (protons and neutrons) are held together by the nuclear mean field potential and strong spin-orbit effect generated by nucleon-nucleon interactions [10,11]. This model has been very successful in describing nuclear properties. On the other hand, "clustering" is a natural energy minimization mechanism. Thus, a question that naturally arises is whether there is any cluster structure in nuclear systems. The formation of structures inside a nucleus is an intriguing phenomenon driven in part by correlations arising from the details of the nucleon-nucleon interaction. With the advance of experimental techniques, recent studies have discovered that some nuclei behave like molecules composed of clusters. Among the different partitioning possibilities within a given nucleus, α-clustering has always been considered the most favorable due to the large binding energy of the α-particle and its inert character. In the present work, we investigate the elastic scattering data for two nuclear systems: the ^{15}N + ^{27}Al system at laboratory energies $E_{lab} = 32.82$, 47.91, 62.07, and 69.84 MeV [6], and the ^{15}N + ^{13}C at $E_{lab} = 30$, 32, and 45 MeV [7,8]. Although these data were measured many years ago, they were only investigated from a phenomenological point of view using the optical model potential with a Woods-Saxon (WS) parameterization. In this work, we investigate these two systems using the Cluster folding model to probe the ^{15}N cluster structure as a core of ^{11}B(^{13}C) with a valence $\alpha(d)$ orbiting the core. The manuscript is structured as follows: Section 2 presents details for the prepared cluster folding potentials for the ^{15}N + ^{27}Al and ^{15}N + ^{13}C systems. Results and discussion are given in Sec 3. Section 4 is devoted to the summary of the study.

2. The implemented cluster folding potentials

2.1. Preparing the cluster folding potential for the ^{15}N + ^{27}Al system

The Ikeda diagram [12], proposed in the late 1960s, conveys the idea that the cluster degrees of freedom appear in the vicinity of the alpha emission threshold. In recent decades, more evidence of alpha clustering formation has been found in self-conjugate nuclei [9,13]. Alpha clustering is the key cornerstone towards a complete understanding of the structure of nuclei and fundamental nuclear interactions [14,15]. In favor of the well-known α + ^{11}B cluster structure of ^{15}N, which emerges at an excitation energy of 10.991 MeV, it is of particular interest to construct an interaction potential between the interacting nuclei, ^{15}N and ^{27}Al, that have this underlying structure. Such interaction potential is commonly known as the cluster folding potential (CFP), which can be generated using the cluster folding (CF) procedures described below. The real and imaginary CFPs for the ^{15}N + ^{27}Al system are defined based on α + ^{27}Al and ^{11}B + ^{27}Al potentials as follows:

$$V^{CF}(\mathbf{R}) = \int \left(V_{^{11}\mathrm{B}+^{27}\mathrm{Al}} \left[\mathbf{R} - \frac{4}{15}\mathbf{r} \right] + V_{\alpha+^{27}\mathrm{Al}} \left[\mathbf{R} + \frac{11}{15}\mathbf{r} \right] \right) |\chi_{\alpha+^{11}\mathrm{B}}(\mathbf{r})|^2 d\mathbf{r}, \quad (1)$$

$$W^{CF}(\mathbf{R}) = \int \left(W_{^{11}\mathrm{B}+^{27}\mathrm{Al}} \left[\mathbf{R} - \frac{4}{15}\mathbf{r} \right] + W_{\alpha+^{27}\mathrm{Al}} \left[\mathbf{R} + \frac{11}{15}\mathbf{r} \right] \right) |\chi_{\alpha+^{11}\mathrm{B}}(\mathbf{r})|^2 d\mathbf{r}, \quad (2)$$

where $V_{^{11}\mathrm{B}+^{27}\mathrm{Al}}$ and $V_{\alpha+^{27}\mathrm{Al}}$, $W_{^{11}\mathrm{B}+^{27}\mathrm{Al}}$ and $W_{\alpha+^{27}\mathrm{Al}}$ are the real and imaginary parts of the nuclear potentials for the ^{11}B + ^{27}Al and α + ^{27}Al channels, which were prepared using the modified São Paulo potential (SPP2) [16] at energies $E(^{11}\mathrm{B}) \approx 11/15\ E(^{15}\mathrm{N})$, and $E_\alpha \approx 4/15\ E(^{15}\mathrm{N})$, respectively, using the standard normalization factors for the real (N_{RSPP}) and imaginary (N_{ISPP}) São Paulo potential, ($N_{\mathrm{RSPP}} = 1.0$ and $N_{\mathrm{ISPP}} = 0.78$). The SPP is derived by folding the densities of the projectile and target nuclei with an effective interaction potential, ν_{NN}^{SPP2}, which is energy-dependent and expressed as:

$$\nu_{NN}^{SPP2} = (\vec{R}) = -U_0 e^{-(R/a)^2 e^{-4v^2/c^2}}, \quad (3)$$

where $U_0 = 735.813$ MeV, $a = 0.5$ fm, v is the relative velocity between the colliding nuclei, and c is the speed of light. The nuclear densities of α, ^{11}B, and ^{27}Al nuclei were calculated using the Dirac-Hartree-Bogoliubov (DHB) model [17] with the REGINA code. The wave function, which describes the relative motion of α and ^{11}B in the ground state of ^{15}N, was calculated using the standard "well-depth" procedure. This function represents a $2D_2$ state in a real WS potential with geometrical parameters fm and $a = 0.65$ fm), and a depth $V_0 = 38.95$ MeV, which was varied so that the binding energy of the cluster could be reached. The generated real and imaginary CFPs for the ^{15}N + ^{27}Al system at $E_{lab} = 32.82$, 47.91, 62.07, and 69.84 MeV, while energy-dependent, do not vary appreciably over the considered energy range, as depicted in Fig. 1.

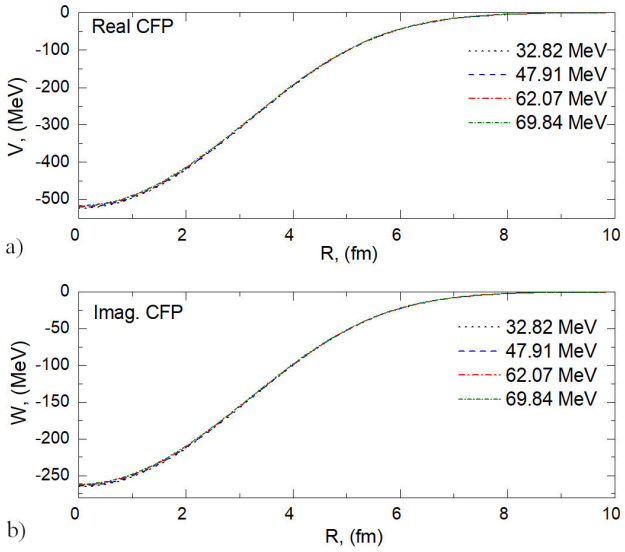

FIGURE 1. Real and imaginary CFPs for the ^{15}N + ^{27}Al system at $E_{lab} = 32.82$, 47.91, 62.07, and 69.84 MeV.

2.2. Preparing the cluster folding potential for the ^{15}N + ^{13}C system

For investigating the ^{15}N + ^{13}C system, the well-known d + ^{13}C cluster structure of ^{15}N, which emerges at an excitation energy of 16.159 MeV, was considered to generate the CFP between the interacting ^{15}N and ^{13}C nuclei. The ^{15}N + ^{13}C CFP is prepared using the CF procedures described below. The real and imaginary CFPs for the ^{15}N + ^{13}C system are defined based on d + ^{13}C and ^{13}C + ^{13}C potentials as follows:

$$V^{CF}(\mathbf{R}) = \int \left(V_{^{13}\mathrm{C}+^{13}\mathrm{C}} \left[\mathbf{R} - \frac{2}{15}\mathbf{r} \right] + V_{d+^{13}\mathrm{C}} \left[\mathbf{R} + \frac{13}{15}\mathbf{r} \right] \right) |\chi_{d+^{13}\mathrm{C}}(\mathbf{r})|^2 d\mathbf{r}, \quad (4)$$

$$W^{CF}(\mathbf{R}) = \int \left(W_{^{13}\mathrm{C}+^{13}\mathrm{C}} \left[\mathbf{R} - \frac{2}{15}\mathbf{r} \right] + W_{d+^{13}\mathrm{C}} \left[\mathbf{R} + \frac{13}{15}\mathbf{r} \right] \right) |\chi_{d+^{13}\mathrm{C}}(\mathbf{r})|^2 d\mathbf{r}, \quad (5)$$

where $V_{^{13}\mathrm{C}+^{13}\mathrm{C}}$ and $V_{d+^{13}\mathrm{C}}$ and $W_{^{13}\mathrm{C}+^{13}\mathrm{C}}$ and $W_{d+^{13}\mathrm{C}}$ are the real and imaginary parts of nuclear potentials for $^{13}\mathrm{C} + ^{13}\mathrm{C}$ and $d + ^{13}\mathrm{C}$ channels, which were prepared using the São Paulo potential (SPP2) [16] at energies $E(^{13}\mathrm{C}) \approx 13/15E(^{15}\mathrm{N})$ and $E_d \approx 2/15E(^{15}\mathrm{N})$, respectively, with

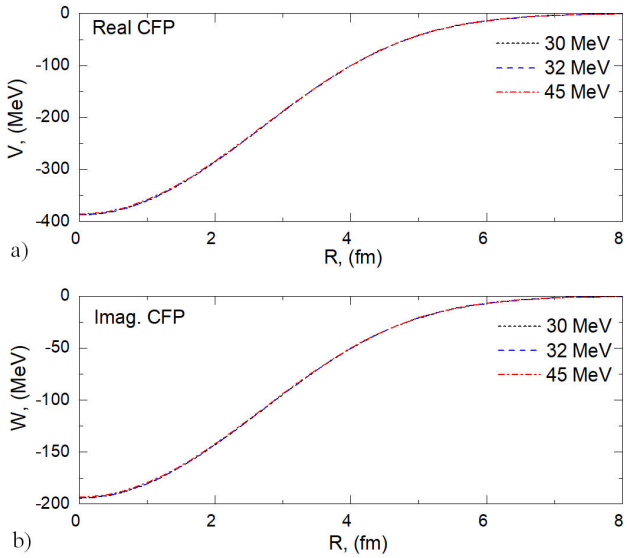

FIGURE 2. Real and imaginary CFPs for the ^{15}N + ^{13}C system at E_{lab} = 30, 32, and 45 MeV.

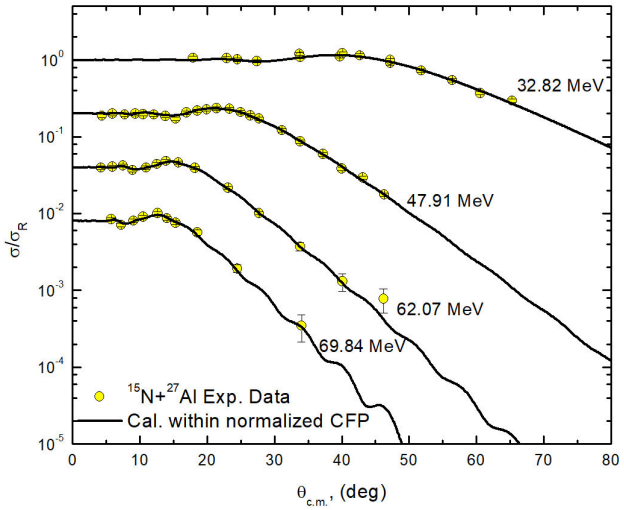

FIGURE 3. The experimental ^{15}N + ^{27}Al ADs versus the theoretical calculations within the CFP framework (solid curves) at E_{lab} = 32.82, 47.91, 62.07, and 69.84 MeV based on the α + ^{11}B cluster structure for ^{15}N. Data are displaced by 0.2 for the sake of clarity.

standard normalization factors for the real (N_{RSPP}) and imaginary (N_{ISPP}) São Paulo potential, ($N_{RSPP} = 1.0$ and $N_{ISPP} = 0.78$). The nuclear densities of d and ^{13}C nuclei were calculated using the DHB model [17] with the REGINA code. The wave function, which describes the relative motion of d and ^{13}N in the ground state of ^{15}N, was calculated using the standard "well-depth" procedure. This function represents a 2S1 state in a real WS potential with geometrical parameters ($R = 1.25 \times [2^{1/3} + 13^{1/3}]$ fm and $a = 0.65$ fm), and a depth $V_0 = 40.54$ MeV, which was varied until the reaching of the binding energy of the cluster. The generated real and imaginary CFPs for the ^{15}N + ^{13}N system at E_{lab} = 30, 32, and 45 MeV are depicted in Fig. 2.

3. Results and discussions

3.1. Analysis of ^{15}N + ^{27}Al ADs within CFM based on the α + 11B cluster structure of ^{15}N

The ^{15}N + ^{27}Al elastic scattering ADs at E_{lab} = 32.82, 47.91, 62.07, and 69.84 MeV [6] are analyzed microscopically using the CFP based on the α + ^{11}B cluster structure for ^{15}N using Eqs. (1) and (2). The implemented potential has the form:

$$U(R) = V_c(R) - N_{RCF}V^{CF}(r) - iN_{ICF}W^{CF}(r), \quad (6)$$

where $V_c(R)$ is the Coulomb potential, characterized by radius $R_C = r_C(A_p^{1/3} + A_t^{1/3})$, $R_C = 1.3$ fm. The theoretical computations within the CFP framework were carried out using two adjustable parameters, N_{RCF} and N_{ICF}, which are factors for renormalizing the real, $V^{CF}(R)$, and imaginary, $W^{CF}(R)$, CFPs, respectively. The optimally extracted N_{RCF} and N_{ICF} values for the different energies involved are listed in Table I. The theoretical computations within the CFP framework agree reasonably well with the experimental ^{15}N + ^{27}Al ADs, as shown in Fig. 3. An important finding from the investigation is the need to reduce the real and imaginary CFP strengths by about 48% and 25%, respectively. The results of the current analyses were obtained within the FRESCO and SFRESCO search codes [18].

Furthermore, the real (J_V) and imaginary (J_W) volume integrals, which are commonly utilized within optical model potentials to characterize the interaction between two nuclei, were calculated. These integrals are crucial for understanding scattering processes. The quantity J_V denotes the non-

TABLE I. The optimal N_{RCF} and N_{ICF} values extracted from the theoretical analysis for the ^{15}N + ^{27}Al system within the normalized CFP. Values of reaction cross section (σR) as well as J_V and J_W values are also listed.

E (MeV)	N_{RCF}	N_{ICF}	$\chi^{2/N}$	σ_R (mb)	J_V (MeV·fm^3)	J_W (MeV·fm^3)
32.82	0.468	0.534	1.07	849.3	195.69	113.49
47.91	0.493	0.764	0.70	1365	204.69	161.25
62.07	0.508	0.865	0.28	1599	209.53	181.38
69.84	0.598	0.839	0.64	1678	245.76	175.30

TABLE II. The optimal N_{RCF} and N_{ICF} values extracted from the theoretical analysis for the ^{15}N + ^{13}C system within the normalized CFP. The employed SA_0 and SA_2 values for the configuration ^{15}N→^{13}C $+d$ are given. The σR, J_V, and J_W values are also listed.

E (MeV)		N_{RCF}	N_{ICF}	SA_0	SA_2	χ^2/N	σ_R (mb)	J_V (MeV·fm^3)	J_W (MeV·fm^3)
30	CFP	1.155	2.056			7.6	1272	495.58	441.59
	CFP+DWBA	1.155	2.056	0.248*	0.752	33.9	1271		
32	CFP	0.677	1.163			7.4	1164	290.21	249.46
	CFP+DWBA	0.677	1.163	0.248*	0.652	35.9	1162		
45	CFP	1.092	0.145			35.2	1258	465.28	30.92
	CFP+DWBA	1.092	0.145	0.248*	0.817	10.3	1249		

absorptive aspect of the potential, whereas J_W accounts for the absorptive part, quantifying the damping or absorption of the projectile wave function as it interacts with the target nucleus. The real/imaginary volume integral is determined by integrating the real/imaginary part of the potential over the nuclear volume. The extracted J_V values fall within the range 195.69-245.76 MeV·fm^3, which are comparable to previously derived values of 188.71-233.07 MeV·fm^3 for the ^{14}N + ^{27}Al system [19]. Conversely, the extracted JW values for the ^{15}N + ^{27}Al system from the present analysis, ranging from 113.49-181.38 MeV·fm^3, exceed previously reported values of 6.64-85.92 MeV·fm^3 for the ^{14}N + ^{27}Al system [19], indicating a higher degree of absorptivity in the ^{15}N + ^{27}Al system compared to the ^{14}N + ^{27}Al system. Notably, a comparison of the ^{15}N + ^{27}Al system with other neighboring systems such as ^{12}C + ^{27}Al, ^{14}N + ^{27}Al, ^{16}O + ^{27}Al [19] reveals similar trends, where the elastic scattering ADs data show that ^{27}Al does not exhibit a threshold anomaly like ^{28}Si due to transfer reaction or other mechanisms, resulting in an increase in the cross-section at backward angles [20].

3.2. Analysis of ^{15}N + ^{13}C ADs within CFM based on the d + ^{13}C cluster structure of ^{15}N

Theoretically, there has been longstanding interest in a phenomenon termed "Anomalous Large Angles Scattering" (ALAS), initially observed through experimental studies revealing an unexpected increase in measured cross sections at large angles, contrary to predictions based on nuclear potential scattering, which anticipated a decrease [21]. Subsequent investigations have focused on elucidating ALAS, recognizing its pronounced sensitivity to the structural characteristics of both the projectile and target nuclei. Particularly intriguing is the exploration of elastic scattering and transfer reactions involving clusterized nuclei at energies proximate to the Coulomb barrier. The Spectroscopic Amplitude (SA) [22], which delineates the overlap between many-body wave functions of the initial and final states, facilitates the examination of nucleon removal. Experimentally, SAs are commonly determined by comparing measured cross sections for nucleon(s) removal to theoretical predictions. Frequently, SA serves to ascertain the involvement of nucleons from specific orbitals in reaction channels during knock-out and pick-up processes, thereby providing estimates of the number of nucleons residing in particular orbitals of the target nucleus. Consequently, the investigation of SA, which is the square of the spectroscopic factor (SF), is crucial in exploring nucleon-nucleon (NN) interactions.

The ^{15}N + ^{13}C elastic scattering ADs at $E_{lab} = 30$, 32, and 45 MeV [7,8] are analyzed microscopically using the CFP constructed based on the d + ^{13}C cluster structure for ^{15}N using Eqs. (4) and (5). The implemented potential has the same form as presented in Eq. (6). The theoretical computations within the CFP framework were carried out using two adjustable parameters, NRCF and NICF, and their optimal extracted values are listed in Table II. The considered ^{15}N + ^{13}C ADs showed a remarkable increase in differential cross sections (DCs) at backward angles, due to the possible contribution of d transfer between the colliding ^{15}N and ^{13}C nuclei. To check such possibility, only forward hemisphere data (angles $> 90°$) were fitted, and the optimal N_{RCF} and N_{ICF} values were extracted. Therefore, the effects from transfer and coupling to other reaction channels, which could affect the potential parameters, were excluded.

To describe the ^{15}N + ^{13}C ADs data in the full angular range, the DWBA method was employed. The two possible configurations for deuteron removal ($L = 0$ and $L = 2$) were considered, resulting in two spectroscopic amplitudes, SA_0 and SA_2, for the configuration ^{15}N → ^{13}C + d. Within the SFRESCO search code [18], a simultaneous search for the SA_2 value was performed, while the SA_0 value was fixed at 0.248 in accordance with Rudchick *et al*. [23]. The optimal SA_2 values at the different considered energies are listed in Table II. The analysis showed that the major impact comes from deuteron removal from $L = 2$. The obtained results within the CFP and CFP + DWBA frameworks versus the experimental data for the ^{15}N + ^{13}C system are depicted in Fig. 4. Figure 5 illustrates the variation of χ^2/N with the extracted SA_2 values for the configuration ^{15}N→ ^{13}C + d at the different considered energies. The averaged obtained SA_2 value is 0.74, which is higher than the previously calculated value of 0.444 within the translationally-invariant shell-

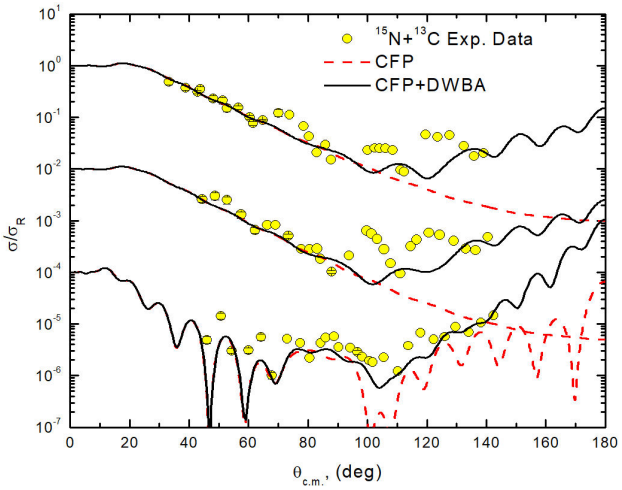

FIGURE 4. The experimental ^{15}N + ^{13}C ADs versus the theoretical calculations within both the CFP framework (dashed red curves) and CFP+DWBA (solid black curves) at E_{lab} = 30, 32, and 45 MeV based on the d + ^{13}C cluster structure for ^{15}N. Data are displaced by 10-2 for clarity.

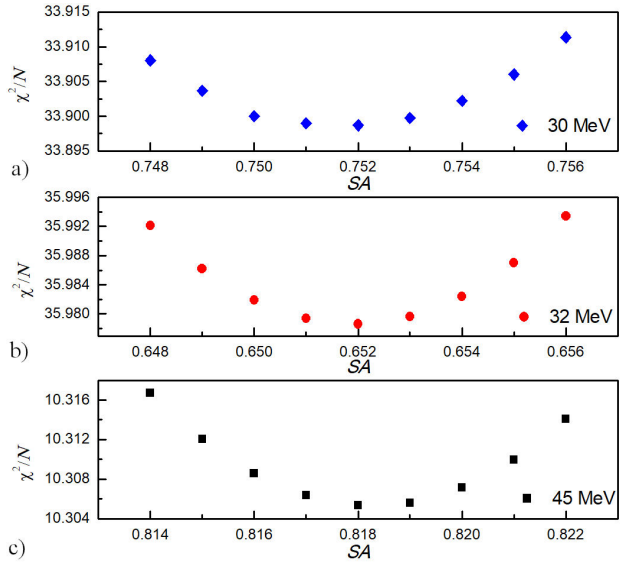

FIGURE 5. Variation of χ^2/N with the extracted SA_2 from the theoretical calculations within the CFP+DWBA framework for the ^{15}N + ^{13}C system at E_{lab} = 30, 32, and 45 MeV.

TABLE III. Cluster quantum numbers (nL_J), binding energies (E_b), and SAs used in the theoretical analyses.

Overlap	nL_J	E_b (MeV)	SA
$\langle^{15}\text{N}\,\vert^{11}\text{B}+\alpha\rangle$	$2D_2$	10.991	0.435 [23]
$\langle^{15}\text{N}\vert^{13}\text{C}+\alpha\rangle$	$2S_1$	16.159	0.248 [23]
	$1D_1$	16.159	0.444 [23]

model [24]. The cluster quantum numbers for the considered overlaps in the present study are presented in Table III and were estimated using the following formula [25]:

$$2(N-1)+L=\sum_{i=1}^{n}2(n_i-1)+l_i, \qquad (7)$$

The analysis of volume integral values extracted for the ^{15}N + ^{13}C system, as presented in Table II, illustrates a trend wherein higher bombarding energies correlate with lower absorptive behavior within the system. It is notable that the derived J_V and J_W values are intricately associated with the normalization factors N_{RCF} and N_{ICF}, respectively, which were determined through the minimization of discrepancies between experimental and calculated differential cross sections.

The analysis of volume integral values extracted for the ^{15}N + ^{13}C system, as presented in Table II, illustrates a trend wherein higher bombarding energies correlate with lower absorptive behavior within the system. It is notable that the derived J_V and J_W values are intricately associated with the normalization factors N_{RCF} and N_{ICF}, respectively, which were determined through the minimization of discrepancies between experimental and calculated differential cross sections.

4. Summary

Studies of nuclear processes induced by clusterized nuclei such as ^{15}N are particularly informative for probing the single-particle structure of nuclei, revealing details about the occupation of nuclear orbitals in both the projectile and target, as well as probing the nuclear structure and dynamics of colliding nuclei. Which sheds light on the interplay between single-particle and collective motions in nuclear systems. In this context, we investigated the scattering of ^{15}N ions on ^{27}Al and ^{13}C targets, within the framework of the cluster folding model, considering the probable ^{11}B +α and ^{13}C + d cluster structures of the ground state of the ^{15}N nucleus. Noteworthy agreement between the measured and calculated ADs data for the considered nuclear systems was achieved, thereby validating the cluster structure depiction of the ^{15}N ground state, conceptualized as a core (^{11}B/^{13}C) with a valence particle (α/d) orbiting the core. The analysis of the ^{15}N + ^{27}Al ADs data emphasized that ^{27}Al has no threshold anomaly, while the ^{15}N + ^{13}C system exhibited a pronounced increase in cross sections at backward angles due to the contribution of d transfer between the colliding nuclei. In comparison with the neighboring system, the ^{15}N + ^{27}Al showed strong absorption, which is reflected in the extracted JW values. The average SA for the ^{15}N$\rightarrow^{13}$C+d cluster configuration was extracted and compared to the previously reported value [23].

Acknowledgments

This research has been funded by the Science Committee of the Ministry of Science and Higher Education of the Republic of Kazakhstan (Grant No. AP13268907).

1. N. Amangeldi *et al.*, Recent Measurement and Theoretical Analysis for the Elastic Scattering of the ^{15}N+^{11}B System, *Braz. J. Phys.* **54** (2024) 169, https://doi.org/10.1007/s13538-024-01547-2.
2. N. Burtebayev *et al.*, Scattering of ^{15}N Ions by ^{10,11}B Nuclei at the Energy of 43 MeV, *Acta Physica Polonica B. Proc.* **11** (2018) 99, https://doi.org/10.5506/APhysPolBSupp.11.99.
3. A.T. Rudchik *et al*., ^{15}N elastic and inelastic scattering by ^{11}B at 84 MeV *Nucl. Phys. A* **939** (2015) 1, https://doi.org/10.1016/j.nuclphysa.2015.02.006.
4. N. Burtebayev *et al*., Elastic scattering of ^{15}N ions by ^{16}O at the energy 11.59 MeV, *Acta Physica Polonica B* **48** (2017) 495, https://doi.org/10.5506/APhysPolB.48.495.
5. A.T. Rudchik *et al.*, Elastic and inelastic scattering of ^{15}N ions by ^{9}Be at 84 MeV *Nucl. Phys. A* **947** (2016) 161, https://doi.org/10.1016/j.nuclphysa.2016.01.002.
6. F. W. Prosser *et al.*, Complete fusion of ^{15}N+^{27}Al, *Phys. Rev. C* **21** (1980) 1819, https://doi.org/10.1103/PhysRevC.21.1819.
7. A. Gamp *et al.*, Interfering proton and neutron transfer in the reaction ^{13}C(^{15}N, ^{14}N)^{14}C *Nucl. Phys. A* **250** (1975) 341, https://doi.org/10.1016/0375-9474(75)90264-X.
8. A. T. Rudchik *et al.*, Elastic and inelastic scattering of ^{15}N ions by ^{13}C nuclei at energy 84 MeV, *Nucl. Phys. At. Energy* **22** (2021) 10, https://doi.org/10.15407/jnpae2021.01.010.
9. M. Freer, The clustered nucleus-cluster structures in stable and unstable nuclei, *Rep. Prog. Phys.* **70** (2007) 2149, https://doi.org/10.1088/0034-4885/70/12/R03.
10. M. G. Mayer, On Closed Shells in Nuclei. II, *Phys. Rev.* **75** (1949) 1969, https://doi.org/10.1103/PhysRev.75.1969.
11. O. Haxel, J. H. D. Jensen, and H. E. Suess, The Systematic Structure-Change into the Molecule-like Structures in the Self-Conjugate 4n Nuclei, *Phys. Rev.* **75** (1949) 1766, https://doi.org/10.1103/PhysRev.75.1766.2.
12. K. Ikeda, N. Takigawa, and H. Horiuchi, Nuclear clusters and nuclear molecules, *Prog. Theor. Phys. Suppl. E* **68** (1968) 464, https://doi.org/10.1143/PTPS.E68.464.
13. W. von. Oertzen, M. Freer, and Y. Kanada-En'yo, Nucleons come together, *Phys. Rep.* **432** (2006) 43, https://doi.org/10.1016/j.physrep.2006.07.001.
14. M. Freer, How atomic nuclei cluster, *Nature* **487** (2012) 309, https://doi.org/10.1038/487309a.
15. J.-P. Ebran, E. Khan, T. Nikšić, and D. Vretenar, São Paulo potential version 2 (SPP2) and Brazilian nuclear potential (BNP), *Nature* **487** (2012) 341, https://doi.org/10.1038/nature11246.
16. L. C. Chamon, B. V. Carlson and L. R. Gasques, Dirac-Hartree-Bogoliubov approximation for finite nuclei, *Comp. Phys. Comm*. **267** (2021) 108061, https://doi.org/10.1016/j.cpc.2021.108061.
17. B.V. Carlson and D. Hirata, Coupled reaction channels calculations in nuclear physics, *Phys. Rev. C* **62** (2000) 054310, https://doi.org/10.1103/PhysRevC.62.054310.
18. I. J. Thompson, *Comput. Phys. Rep.* **7** (1988) 167. https://doi.org/10.1016/0167-7977(88)90005-6.
19. Sh. Hamada, N Burtebayev, K A Gridnev, N Amangeldi, Further investigation of the elastic scattering of ^{16}O, ^{14}N and ^{12}C on the nucleus of ^{27}Al at low energies, *Phys. Scr.* **84** (2011) 045201, https://doi.org/10.1088/0031-8949/84/04/045201.
20. M. A. Franey, V. Shkolnik, D. Dehnhard, Elastic transfer in the scattering of ^{16}O by ^{28}Si, *Phys. Lett. B* **81** (1979) 132, https://doi.org/10.1016/0370-2693(79)90505-7.
21. S. Szilner, W. Von Oertzen, Z. Basrak, F. Haas, M. Milin, Elastic α-transfer in the elastic scattering of ^{16}O + ^{12}C *Eur. Phys. J. A.* **13** (2002) 273, https://doi.org/10.1007/s10050-002-8754-9.
22. B. A. Brown, A. Csoto and R. Sherr, Coulomb displacement energy and the low-energy astrophysical S_{17} factor for the ^{7}Be(p,γ)8B reaction, *Nucl. Phys. A* **597** (1996) 66, https://doi.org/10.1016/0375-9474(95)00417-3.
23. A. A. Rudchik *et al*., Mechanism of the ^{12}C(^{11}B,^{15}N)^{8}Be reaction and 8Be + ^{15}N optical-model potential, *Eur. Phys. J. A* **23** (2005) 445, https://doi.org/10.1140/epja/i2004-10100-3.
24. Yu. F. Smirnov, Yu.M. Tchuvil'sky, Cluster spectroscopic factors for the *p*-shell nuclei, *Phys. Rev. C* **15** (1977) 84, https://doi.org/10.1103/PhysRevC.15.84.
25. B. Buck and A. A. Pilt, Alpha-particle and triton cluster states in ^{19}F, *Nucl. Phys. A* **280** (1977) 133, https://doi.org/10.1016/0375-9474(77)90300-1.